Title: Poster Advertisement Session

Date: Jun 26, 2010 02:30 PM

URL: http://pirsa.org/10060091

Abstract: N/A

Notes on the integration of numerical relativity waveforms

Christian Reisswig & Denis Pollney

NRDA 2010

06/2010

Motivation

Computation of the strain *h*

- The gravitational strain, h, is the quantity that gravitational-wave detectors measure.
- Most NR computations **do not directly** compute h.
- Instead, the complex Weyl component ψ_4 is often used:

$$h = h_+ - ih_\times = \int_{-\infty}^{t} dt' \int_{-\infty}^{t'} dt'' \psi_4 \, . \qquad (1)$$

- Unfortunately, integrating twice in time introduces **spurious drifts**.

Motivation

Computation of the strain h

- The effect is shown below for the $(\ell, m) = (4, 4)$ wavemode of an equal-mass non-spinning binary black hole merger.

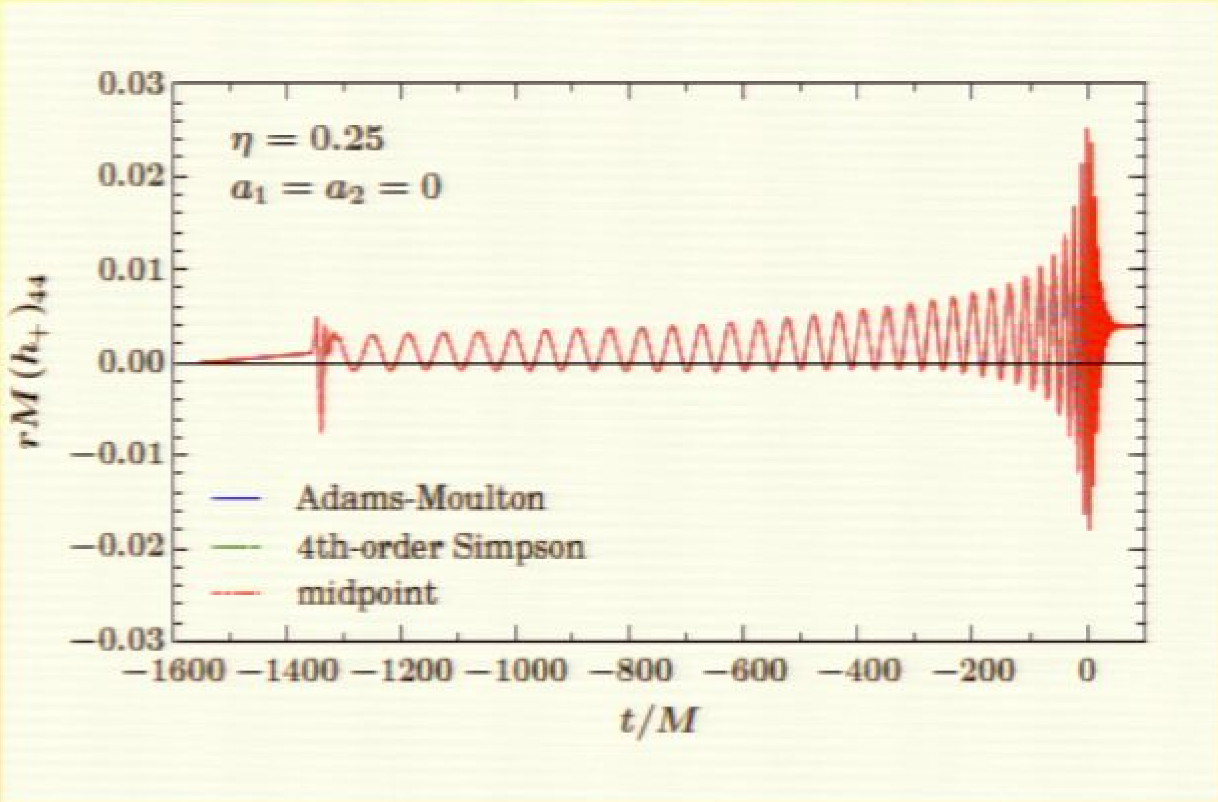

- This drift is **independent of the integration method** used.
- This drift is **not a gauge- or finite radius effect**: the wavemode above has been extracted at future null infinity $\mathcal{J}^+$.

The problem

Computation of the strain *h*

- We identify two different sources of the problem:
  - In time domain, numerical noise induces a **random walk**.
  - In Fourier domain, finite length of the signal causes **spectral leakage**.

Fixed frequency integration

Fixed-frequency integration

- We suggest the following scheme:

$$\tilde{F}(\omega) = \begin{cases} i\tilde{f}(\omega)/\omega_0\,, & \omega \leq \omega_0\,, \\ i\tilde{f}(\omega)/\omega\,, & \omega > \omega_0\,. \end{cases} \tag{2}$$

  where ω_0 smaller than the lowest physical frequency component.

- For binary black holes $\omega_0 \leq \omega_{\mathrm{ini}}$.
- Higher modes: $\omega_0^{\ell m} = \omega_0^{22} m/2$.

Fixed frequency integration

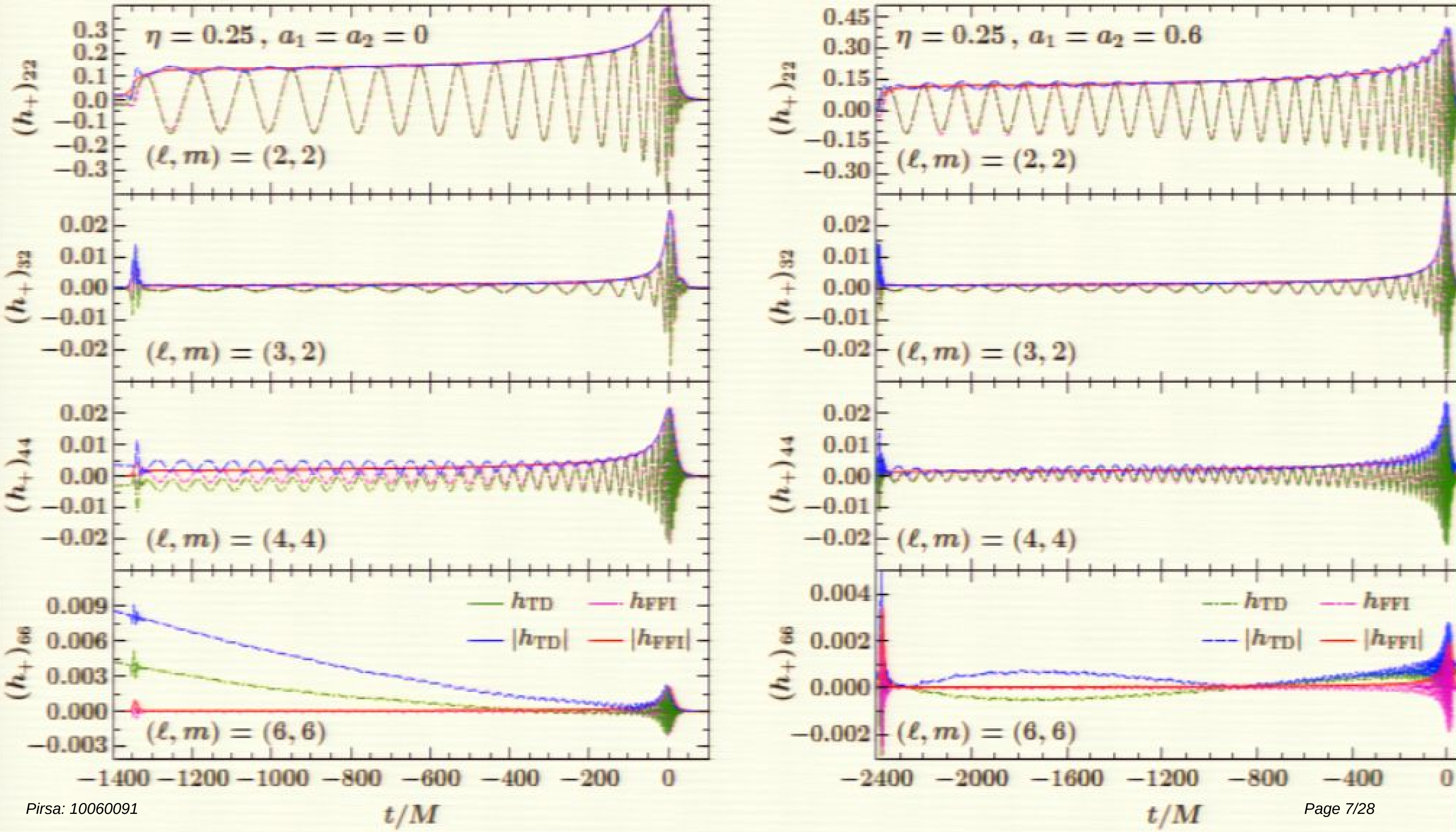

Fixed frequency integration

Further details on the **poster** and in Reisswig & Pollney arXiv:1006.1632

Fixed frequency integration

Further details on the **poster** and in Reisswig & Pollney arXiv:1006.1632

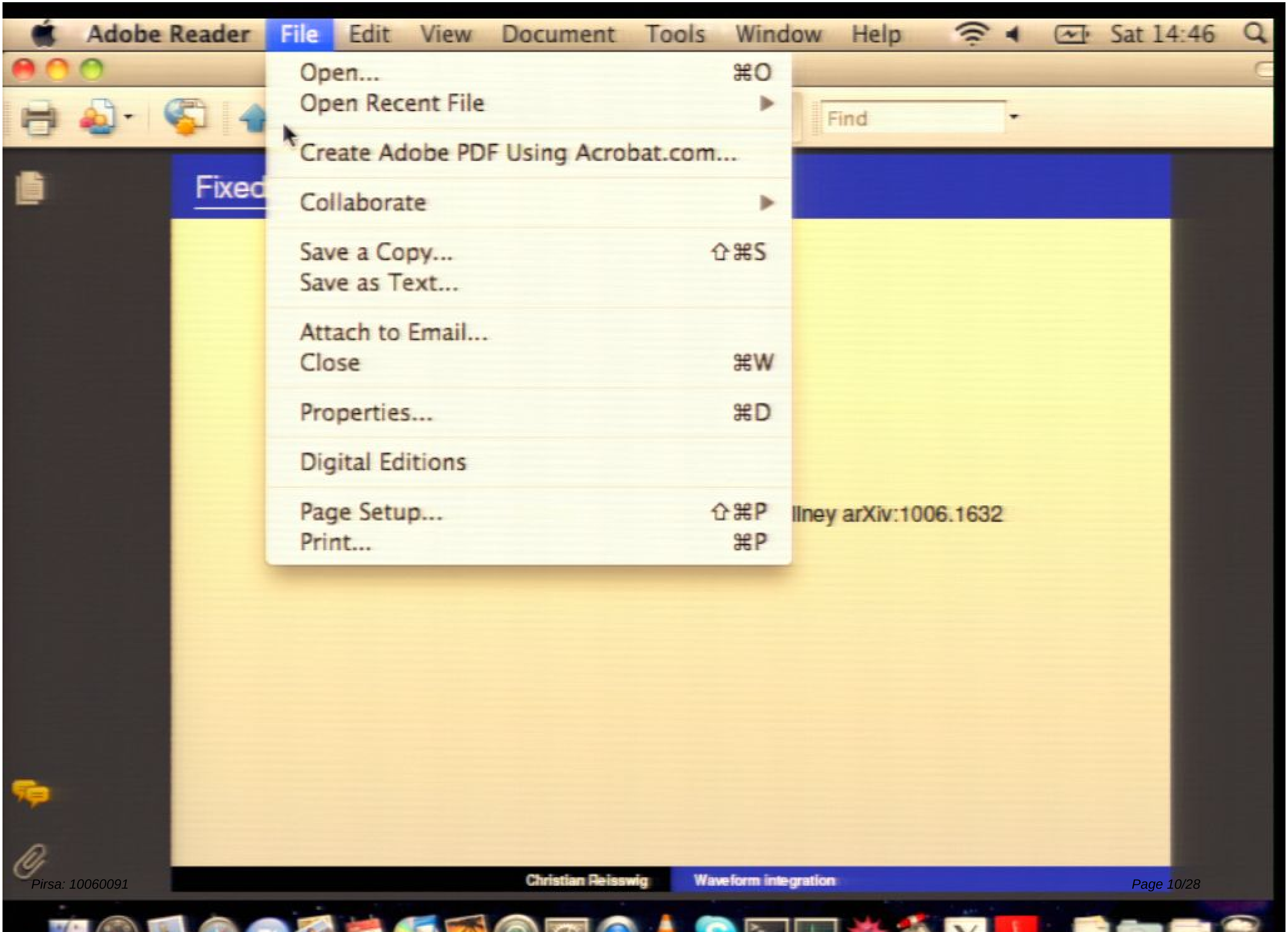
Adobe Reader
File
Edit
View
Document
Tools
Window
Help
Sat 14:46
Find
Fixed
Open... ⌘O
Open Recent File
Create Adobe PDF Using Acrobat.com...
Collaborate
Save a Copy... ⇧⌘S
Save as Text...
Attach to Email...
Close ⌘W
Properties... ⌘D
Digital Editions
Page Setup... ⇧⌘P
Print... ⌘P
llney arXiv:1006.1632
Christian Reisswig
Waveform integration

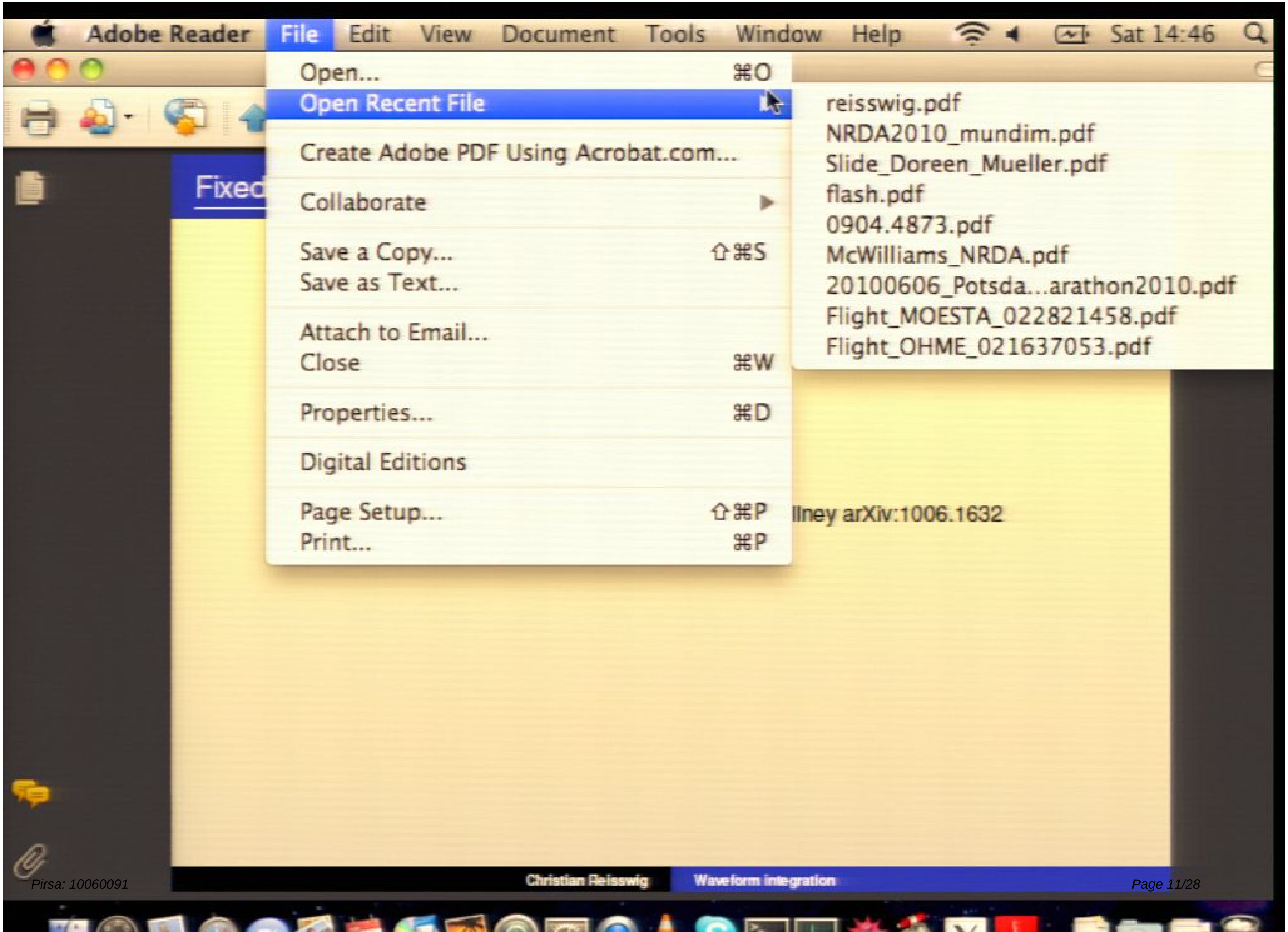
Adobe Reader
File
Edit
View
Document
Tools
Window
Help
Sat 14:46
Open... ⌘O
Open Recent File
Create Adobe PDF Using Acrobat.com...
Collaborate
Save a Copy... ⇧⌘S
Save as Text...
Attach to Email...
Close ⌘W
Properties... ⌘D
Digital Editions
Page Setup... ⇧⌘P
Print... ⌘P
reisswig.pdf
NRDA2010_mundim.pdf
Slide_Doreen_Mueller.pdf
flash.pdf
0904.4873.pdf
McWilliams_NRDA.pdf
20100606_Potsda...arathon2010.pdf
Flight_MOESTA_022821458.pdf
Flight_OHME_021637053.pdf
Fixed
llney arXiv:1006.1632
Christian Reisswig
Waveform integration

Adobe Reader File Edit View Document Tools Window Help Sat 14:46

Slide_Doreen_Mueller.pdf

Bookmarks

NRDA 2010, Perimeter Institute --- Poster presentation

Dynamical shift condition for unequal mass bh binary simulations

$\tilde{\Gamma}$-driver condition

$$\partial_0^2 \beta^i = \frac{3}{4}\partial_0 \tilde{\Gamma}^i - \eta\, \partial_0 \beta^i$$

$$\eta(\vec{r}) = A + \frac{C_1}{1 + w_1 (\hat{r}_1^2)^n} + \frac{C_2}{1 + w_2 (\hat{r}_2^2)^n}$$

with

$$w_i, n > 0$$

$$A = 2/(M_1 + M_2) \quad C_i = 1/M_i - A$$

$$\hat{r}_i = \frac{|\vec{r}_i - \vec{r}|}{|\vec{r}_1 - \vec{r}_2|} \quad (i = 1, 2)$$

$$\eta(\vec{r}) \rightarrow \begin{cases} \dfrac{1}{M_i}, & \vec{r} \rightarrow \vec{r}_i \quad (w_i \gg 1) \\ \dfrac{2}{M_1 + M_2}, & \vec{r} \rightarrow \infty \end{cases}$$

$M_1 = M_2$: $\eta(\vec{r}) = 2/M$ (standard simulations)

- Test system: mass ratio 4:1, $D = 5\,M$
- Results:
  - simulations stable
  - improved amplitude and phase accuracy in 22–mode of Ψ_4 compared to $\eta = \text{const.}$

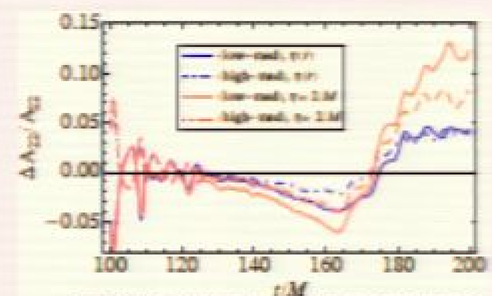

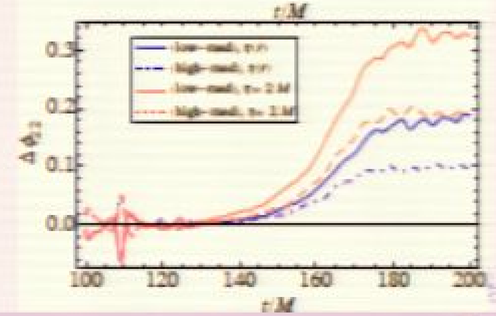

Dynamical shift condition for unequal mass bh binary simulations

$\tilde{\Gamma}$–driver condition

$$\partial_0^2 \beta^i = \frac{3}{4}\partial_0 \tilde{\Gamma}^i - \eta\, \partial_0 \beta^i$$

$$\eta(\vec{r}) = A + \frac{C_1}{1 + w_1\,(\hat{r}_1^2)^n} + \frac{C_2}{1 + w_2\,(\hat{r}_2^2)^n}$$

with $\quad w_i, n > 0$

$$A = 2/(M_1 + M_2) \quad C_i = 1/M_i - A$$

$$\hat{r}_i = \frac{|\vec{r}_i - \vec{r}|}{|\vec{r}_1 - \vec{r}_2|} \qquad (i = 1, 2)$$

$$\eta(\vec{r}) \rightarrow \begin{cases} \dfrac{1}{M_i}, & \vec{r} \rightarrow \vec{r}_i \\ & (w_i \gg 1) \\ \dfrac{2}{M_1 + M_2}, & \vec{r} \rightarrow \infty \end{cases}$$

$M_1 = M_2$: $\eta(\vec{r}) = 2/M$ (standard simulations)

- Test system: mass ratio 4:1, $D = 5\,M$
- Results:
  - simulations stable
  - improved amplitude and phase accuracy in 22–mode of Ψ_4 compared to $\eta = $ const.

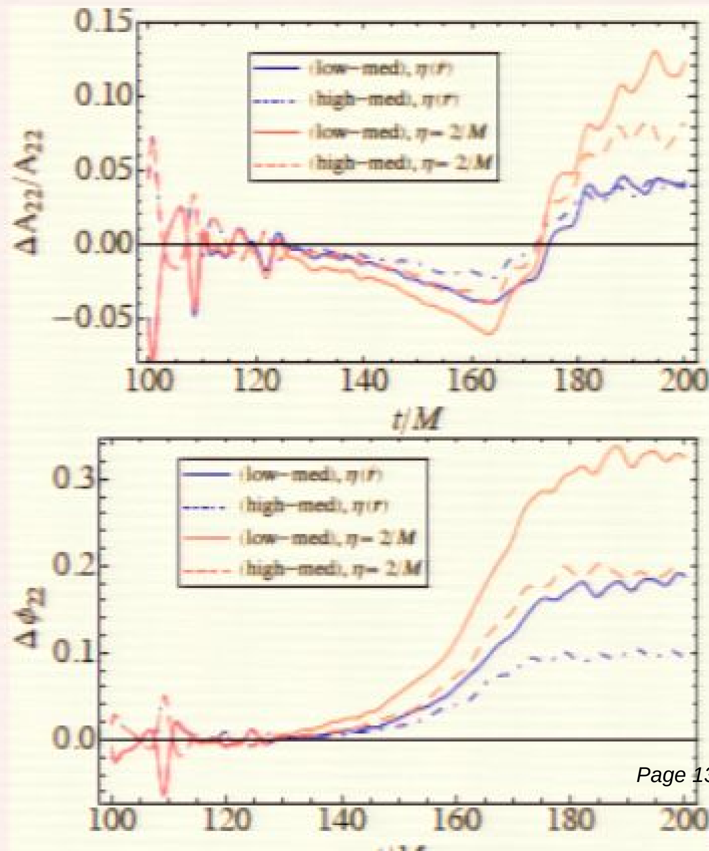

Dynamical shift condition for unequal mass bh binary simulations

$\tilde{\Gamma}$–driver condition

$$\partial_0^2 \beta^i = \frac{3}{4} \partial_0 \tilde{\Gamma}^i - \eta\, \partial_0 \beta^i$$

$$\eta(\vec{r}) = A + \frac{C_1}{1 + w_1\,(\hat{r}_1^2)^n} + \frac{C_2}{1 + w_2\,(\hat{r}_2^2)^n}$$

with $\quad w_i, n > 0$

$$A = 2/(M_1 + M_2) \quad C_i = 1/M_i - A$$

$$\hat{r}_i = \frac{|\vec{r}_i - \vec{r}|}{|\vec{r}_1 - \vec{r}_2|} \qquad (i = 1, 2)$$

$$\eta(\vec{r}) \rightarrow \begin{cases} \dfrac{1}{M_i}, & \vec{r} \rightarrow \vec{r}_i \\ & (w_i \gg 1) \\ \dfrac{2}{M_1 + M_2}, & \vec{r} \rightarrow \infty \end{cases}$$

$M_1 = M_2$: $\eta(\vec{r}) = 2/M$ (standard simulations)

- Test system: mass ratio 4:1, $D = 5\,M$
- Results:
  - simulations stable
  - improved amplitude and phase accuracy in 22–mode of Ψ_4 compared to $\eta = \text{const.}$

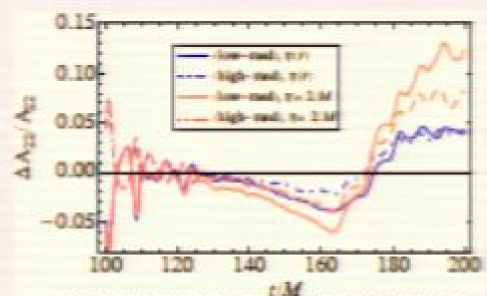

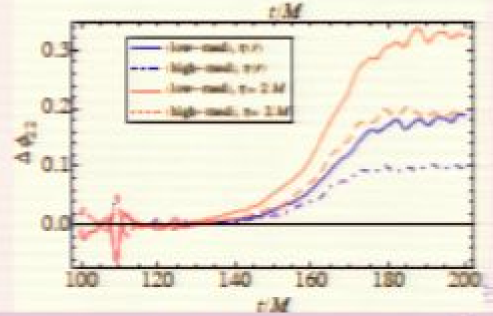

Vacuum electromagnetic counterparts of binary black-hole mergers

Philipp Mösta
Carlos Palenzuela, Luciano Rezzolla, Luis Lehner, Shin'ichirou Yoshida and Denis Pollney

Max-Planck-Institute for Gravitational Physics (Albert-Einstein-Institute)
Am Mühlenberg 1
14476 Potsdam-Golm, Germany

philipp.moesta@aei.mpg.de

June 26, 2010

Vacuum electromagnetic counterparts of binary black-hole mergers

Philipp Mösta
Carlos Palenzuela, Luciano Rezzolla, Luis Lehner, Shin'ichirou Yoshida and Denis Pollney

Max-Planck-Institute for Gravitational Physics (Albert-Einstein-Institute)
Am Mühlenberg 1
14476 Potsdam-Golm, Germany

philipp.moesta@aei.mpg.de

June 26, 2010

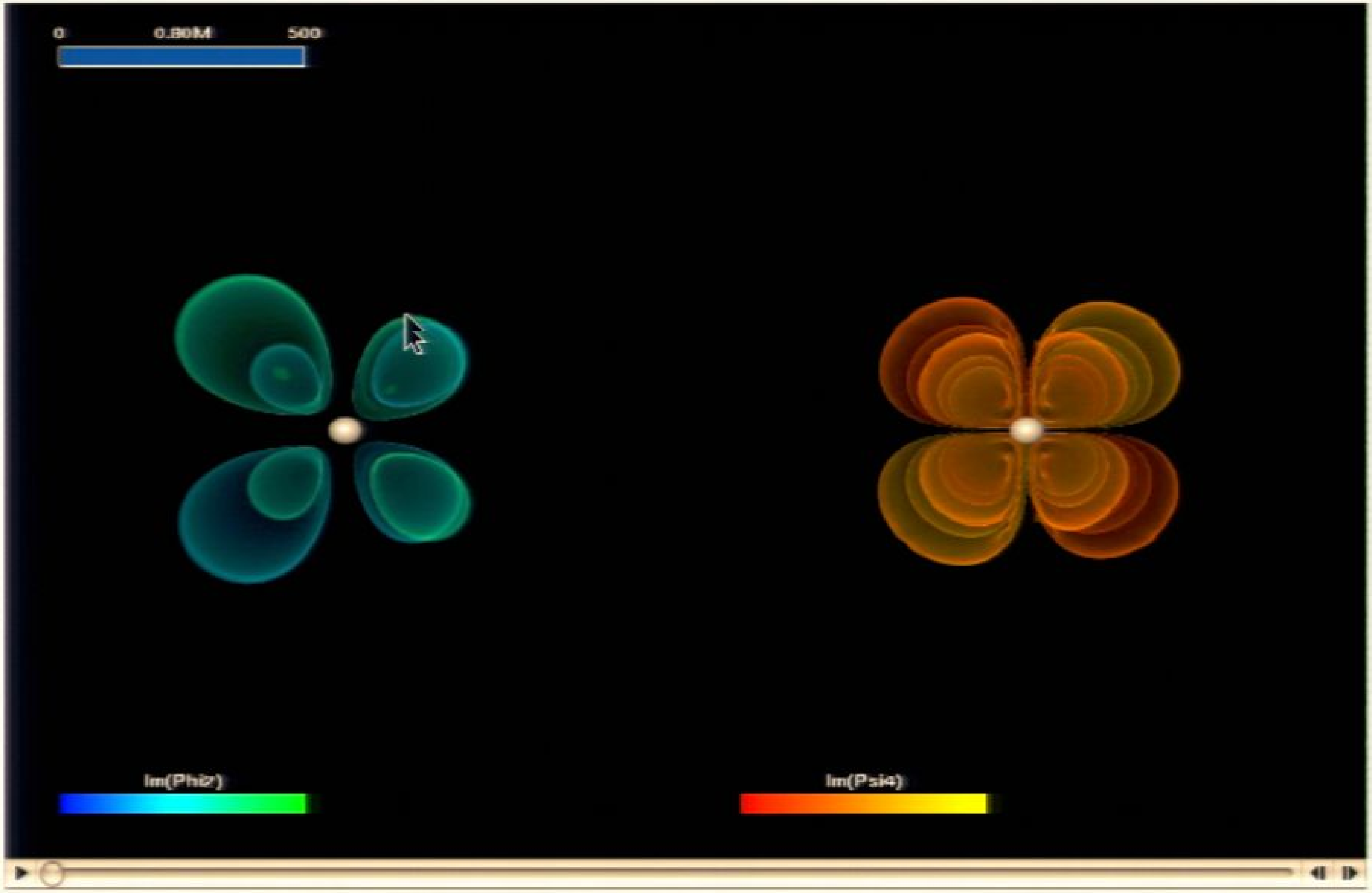
0
0.80M
500
Im(Phi2)
Im(Psi4)

Hybrid black-hole binary initial data

Bruno C. Mundim

Collaborators:

BJ Kelly, Y Zlochower, H Nakano, M Campanelli

Center for Computational Relativity and Gravitation
Rochester Institute of Technology

NRDA - June 26, 2010

Post-Newtonian metric: ADM-TT coordinates

- Tichy *et al* (2003) adapted the 2.5PN ADM-TT results to puncture initial data for numerical relativity.
- We start from the PN expression for the spatial metric:

$$\gamma_{ij}^{PN} = \psi_{PN}^4 \delta_{ij} + h_{ij}^{TT}, \tag{1}$$

- The post-Newtonian expansion for the conjugate momenta is simply:

$$\pi^{ij}_{PN} = \psi_{PN}^{-4} \left(\epsilon^3 \tilde{\pi}^{ij}_{(3)} + \epsilon^5 \tilde{\pi}^{ij}_{(5)} \right) \tag{2}$$

- Advantages of ADM-TT data:
  - 3-metric and extrinsic curvature expressions easily found.
  - No logarithmics divergences (as in the harmonic coordinates).
  - Single BH data reduces to Schwarzschild in isotropic coordinates.
  - Up to 1.5PN the data looks similar to the puncture approach: conformally flat and Bowen-York extrinsic curvature.
  - Extrinsic curvature trace vanishes up to 3PN: Hamiltonian constraint decouples

Realistic gravitational wave content

- What about h_{ij}^{TT}?
- Schäfer (1985) suggested a "near zone" approximation for h_{ij}^{TT}, by splitting the retarded inverse d'Alembertian with an inverse Laplacian:

$$\begin{aligned} h_{ij}^{TT} &= -[\Delta^{-1} + (\Box_{ret}^{-1} - \Delta^{-1})]\delta_{ij}^{TT\,kl}\left[\sum_{a=1}^{N} \frac{p_{ak}\,p_{al}}{m_a}\delta_a + \frac{1}{4}\phi_{,k}^{(2)}\phi_{,l}^{(2)}\right] && (3) \\ &= h_{ij}^{TT\,(NZ)} + h_{ij}^{TT\,(remainder)} + O(\epsilon^5). && (4) \end{aligned}$$

- A few years later, Kelly *et al* (2007) completed the picture for nonspinning black-holes by determining the "remainder" TT term, $h_{ij}^{TT\,(remainder)}$ to 2PN order.
- The structure of the remainder term divides into three segments, according to time of evaluation:

$$h_{ij}^{TT\,(remainder)} = h_{ij}^{TT\,(present)} + h_{ij}^{TT\,(retarded)} + h_{ij}^{TT\,(interval)}. \qquad (5)$$

Numerical implementation: early evolutions

- Initial evolutions carried out with BAM, LazEv and Hahndol moving puncture codes.

- Data show strong eccentricity and apparent horizon mass drops gradually over the course of the inspiral.

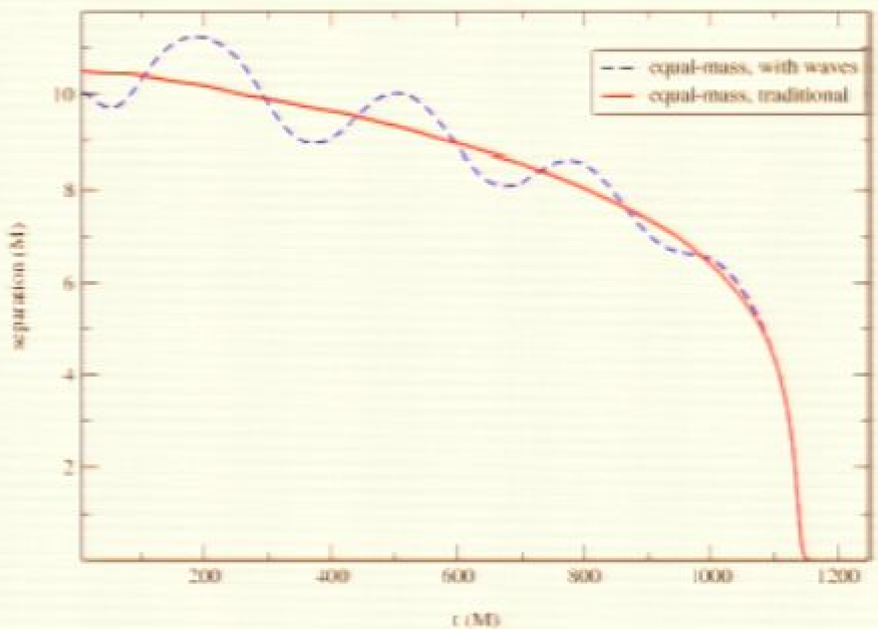

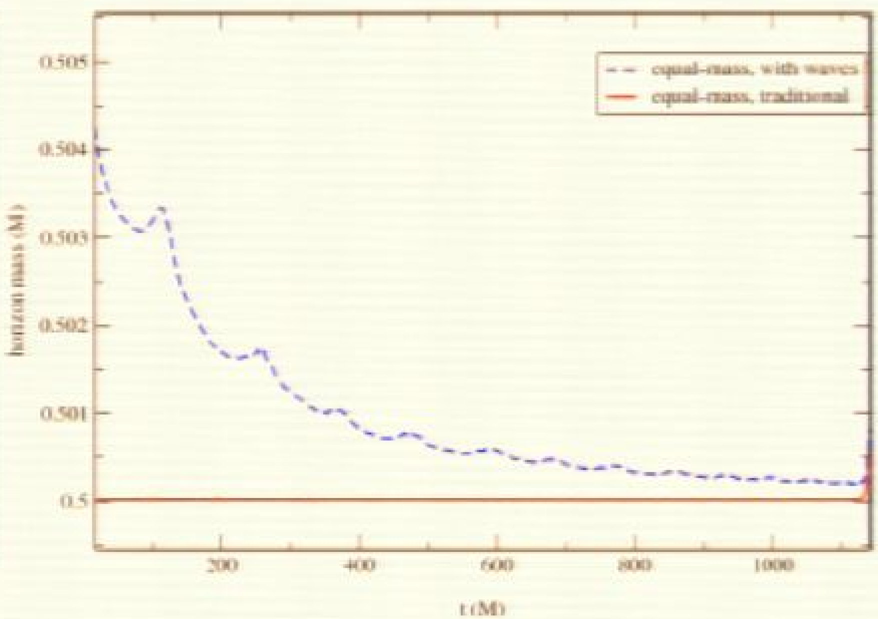

Hybrid initial data

- The largest Hamiltonian violation contributions are due to the ψ_{PN}, since h_{ij}^{TT} is relatively much smaller closer to the punctures.

- Hybrid initial data prescription: solve the Hamiltonian constraint for the traditional Bowen-York puncture initial data and then rescale and superpose the higher order PN terms to this solution:

- The Bowen-York extrinsic curvature is used to source the hamiltonian constraint with conformally flat spatial metric:

$$\Delta\psi_{BY} + K^{ij}_{BY} K^{BY}_{ij} / \psi^7_{BY} = 0, \tag{6}$$

where the solution is $\psi_{BY} = 1 + 1/2(m_1/r_1 + m_2/r_2) + u$. In this new hybrid approach the quantities are rescaled by ψ_{BY} instead of ψ_{PN}:

$$\begin{aligned} \gamma_{ij} &= \psi^4_{BY}\delta_{ij} + h^{TT}_{ij}, & (7)\\ \pi^{ij} &= \frac{1}{\psi^4_{BY}}\left(\pi^{ij}_{(3)} + \pi^{ij}_{(5)}\right). & (8) \end{aligned}$$

and the higher order PN terms, h^{TT}_{ij} and $\pi^{ij}_{(5)}$, superposed to the BY puncture data.

Numerical implementation: current evolutions

- The hybrid initial data approach significantly reduces the unphysical horizon mass loss and Hamiltonian constraint violation observed in evolutions of the wavy ADM-TT PN data.

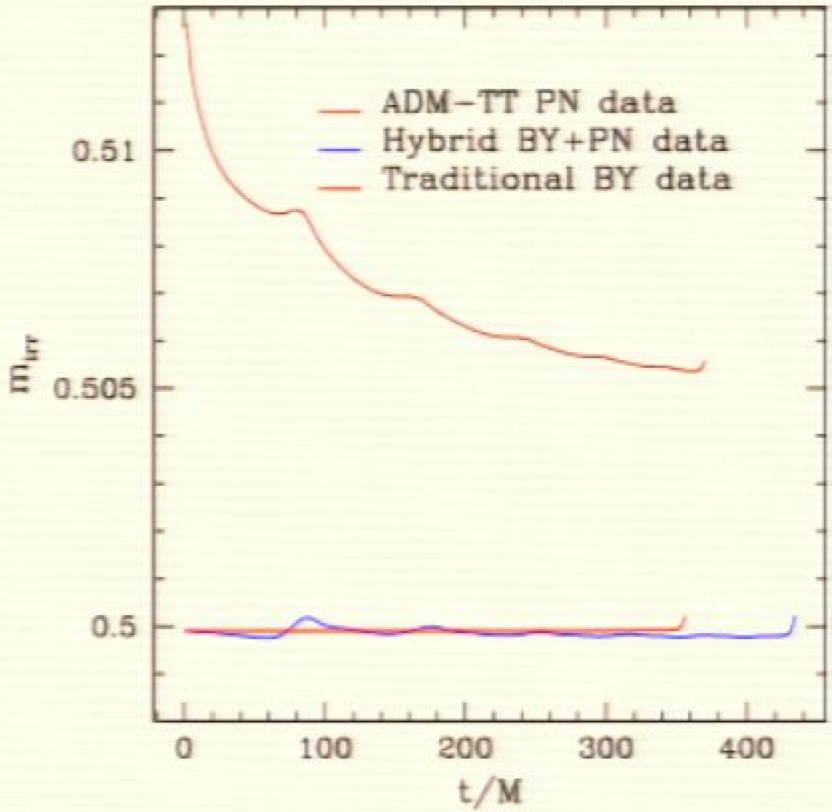

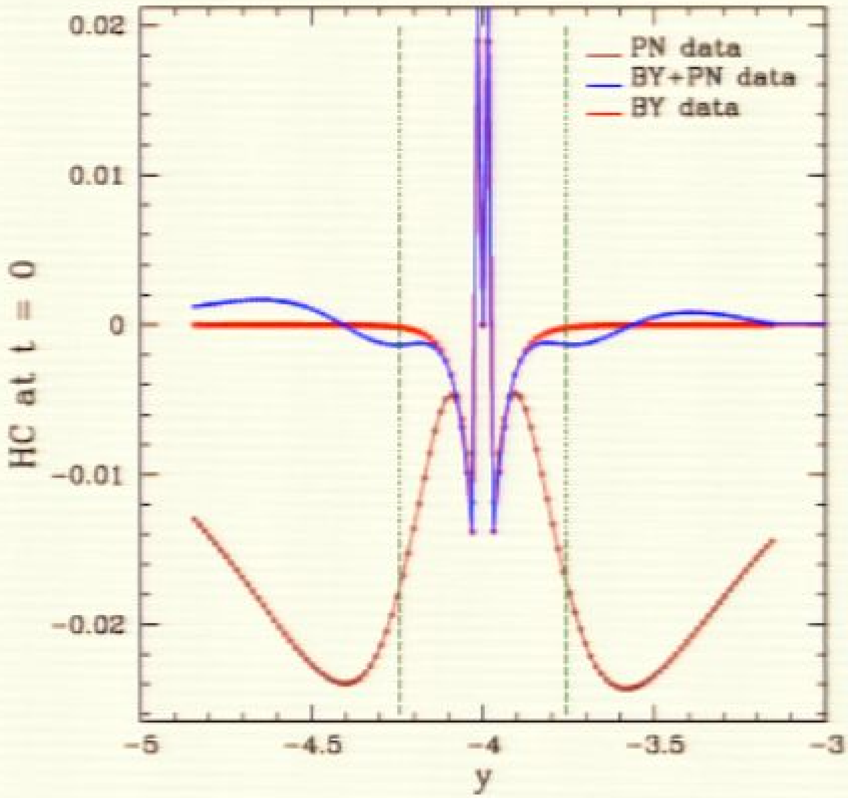

Numerical implementation: current evolutions

- Like the wavy ADM-TT PN data, the hybrid data significantly reduces the amplitude of the spurious radiation when compared to pure BY data.

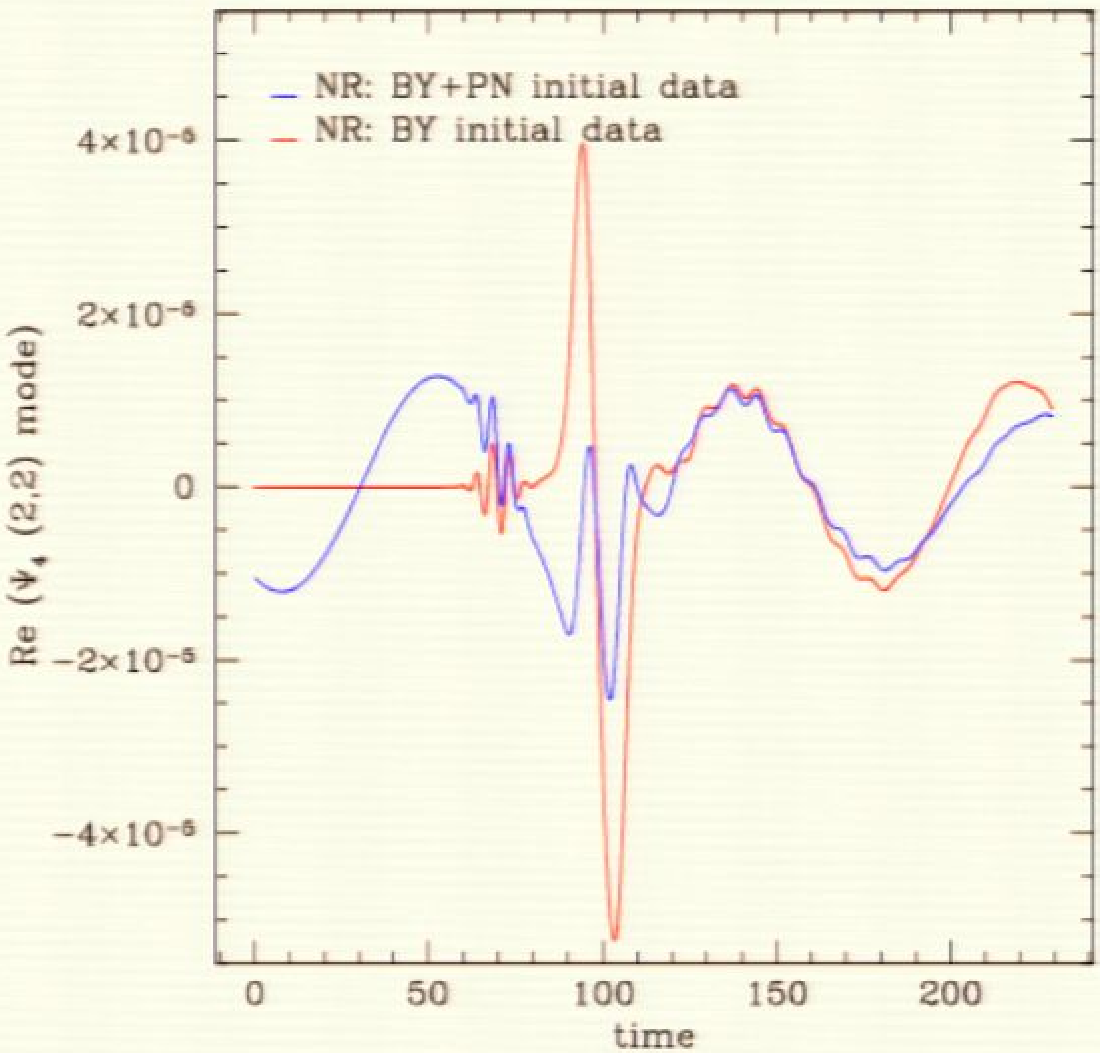

Numerical implementation: current evolutions

- Comparison between PN, BY and BY+PN data. PN and BY+PN waveform amplitude (left) and phase (right) shifted by $36M$ and $77M$, respectively. The extraction radius here is $90M$.

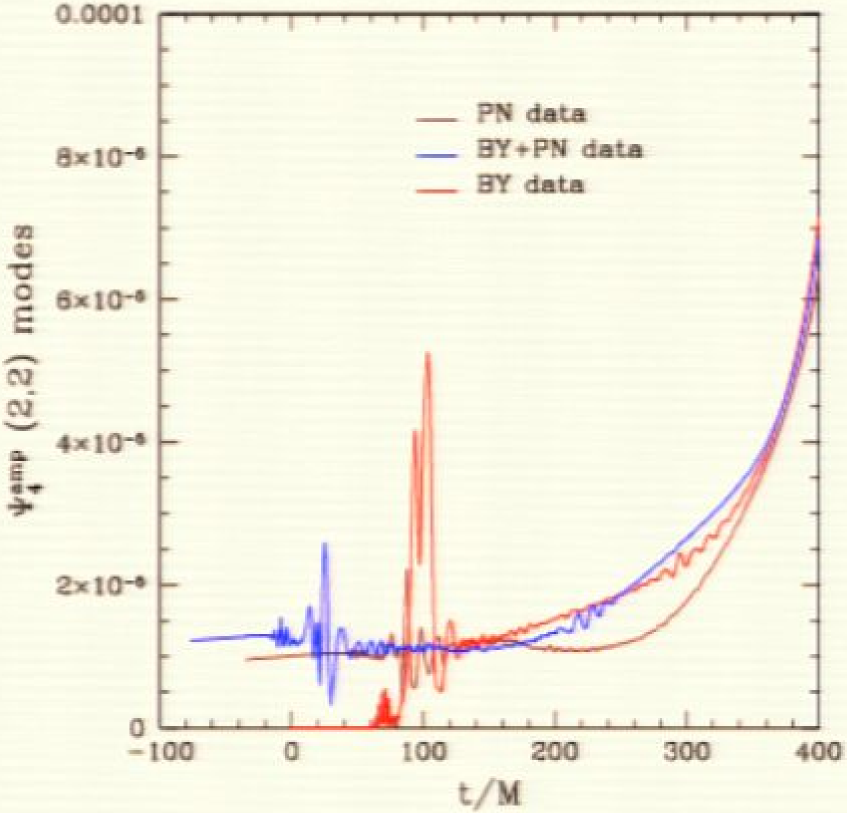

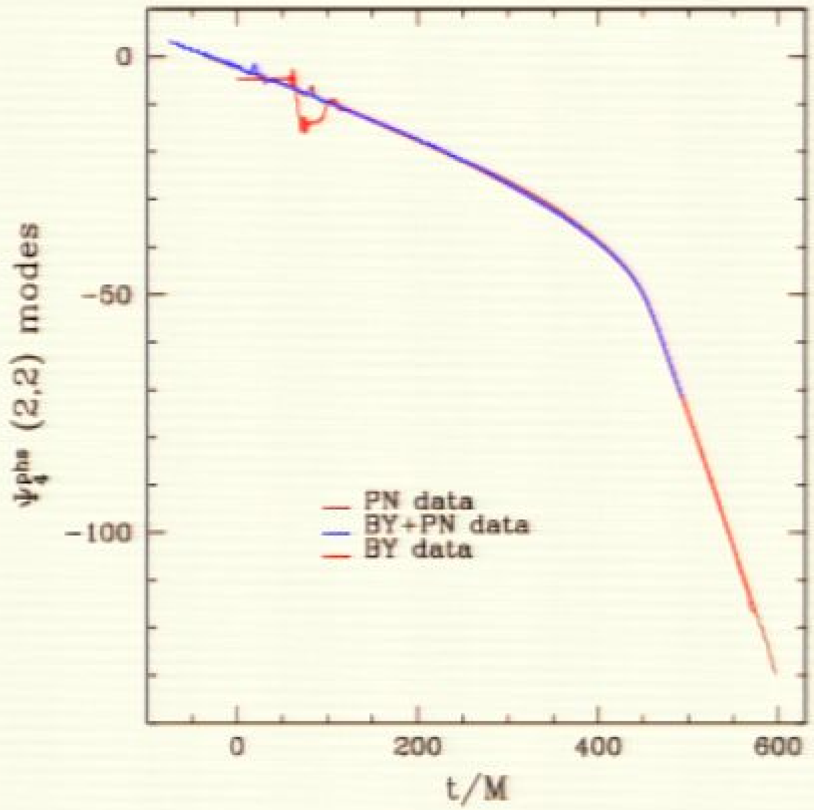

Numerical implementation: current evolutions

- Compare the wavy pattern at $t = 0$ present in $r\,\mathcal{R}e\,(\psi_4)$ for BY+PN initial data (left) with the traditional BY (right) data.

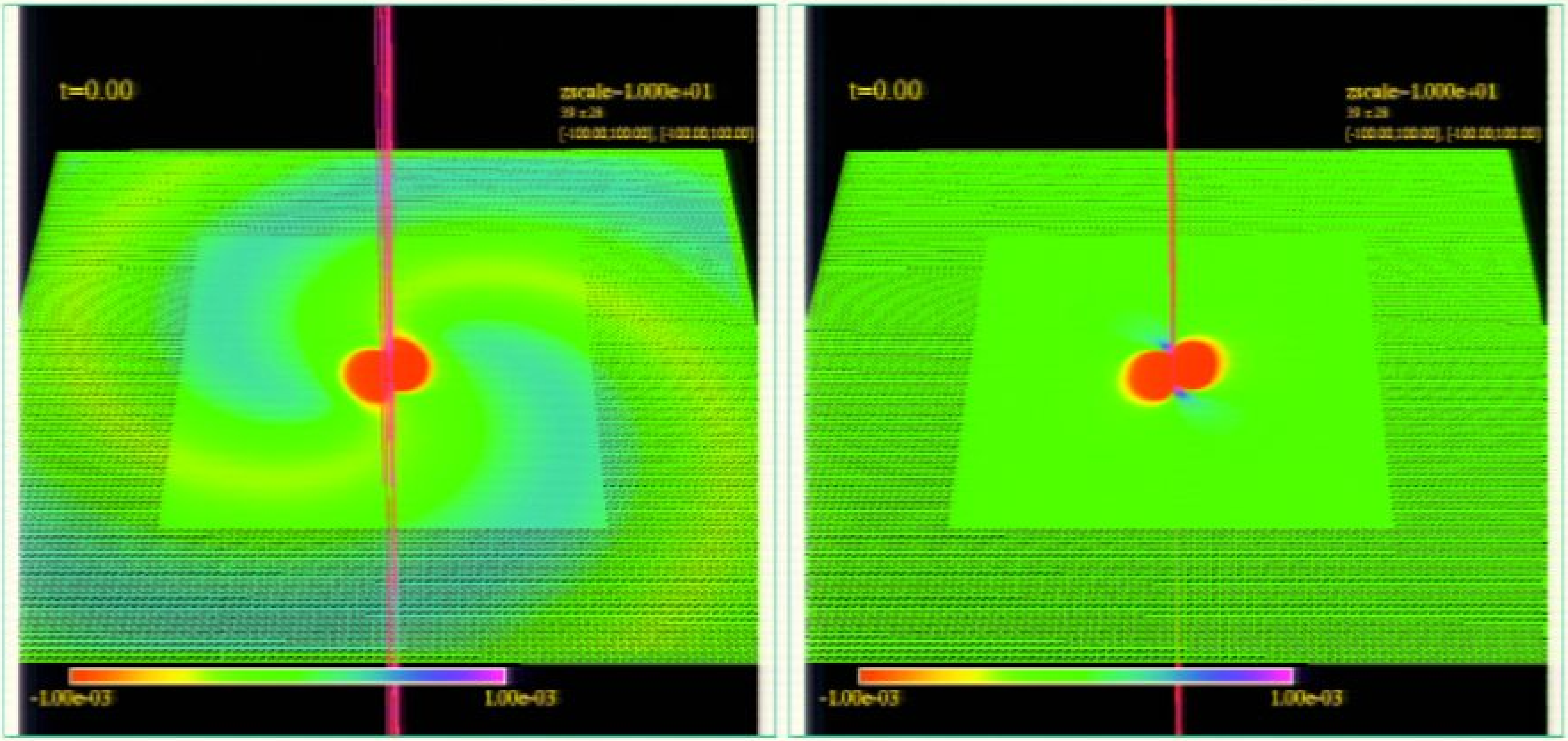

Hybrid BY+PN initial data. Traditional BY initial data.